Boundary-Layer Meteorol
DOI 10.1007/s10546-016-0223-0

RESEARCH ARTICLE

Understanding Diurnality and Inter-Seasonality of a Sub-tropical Urban Heat Island

Tirthankar Chakraborty[1] · **Chandan Sarangi**[2] · **Sachchida Nand Tripathi**[3]

Received: 6 May 2016 / Accepted: 17 November 2016

Abstract We quantify the spatial and temporal aspects of the urban heat-island (UHI) effect for Kanpur, a major city in the humid sub-tropical monsoon climate of the Gangetic basin. Fixed station measurements are used to investigate the diurnality and inter-seasonality in the urban–rural differences in surface temperature (ΔT_s) and air temperature (ΔT_c) separately. The extent of the spatial variations of the nighttime ΔT_c and ΔT_s is investigated through mobile campaigns and satellite remote sensing respectively. Nighttime ΔT_c values dominate during both the pre-monsoon (maximum of 3.6 °C) and the monsoon (maximum of 2.0 °C). However, the diurnality in ΔT_s is different, with higher daytime values during the pre-monsoon, but very little diurnality during the monsoon. The nighttime ΔT_s value is mainly associated with differences in the urban–rural incoming longwave radiative flux ($r^2 = 0.33$ during the pre-monsoon; 0.65 during the monsoon), which, in turn, causes a difference in the outgoing longwave radiative flux. This difference may modulate the nighttime ΔT_c value as suggested by significant correlations ($r^2 = 0.68$ for the pre-monsoon; 0.50 for the monsoon). The magnitude of ΔT_c may also be modulated by advection, as it is inversely related with the urban wind speed. A combination of in situ, remotely sensed, and model simulation data were used to show that the inter-seasonality in ΔT_s, and, to a lesser extent, in ΔT_c, may be related to the change in the land use of the rural site between the pre-monsoon and the monsoon periods. Results suggest that the degree of coupling of ΔT_s and ΔT_c may be a strong function of land use and land cover.

✉ Sachchida Nand Tripathi
snt@iitk.ac.in

Tirthankar Chakraborty
tirthankar25@gmail.com

Chandan Sarangi
chandans@iitk.ac.in

1 Environmental Engineering and Management Programme, IIT Kanpur, Kanpur, India

2 Civil Engineering Department, IIT Kanpur, Kanpur, India

3 Civil Engineering Department and Centre for Environmental Science & Engineering, IIT Kanpur, Kanpur, India

Published online: 20 December 2016

Keywords Land-surface model · Land-surface temperature · Radiative balance · Remote sensing · Urban heat-islands

1 Introduction

The urban heat-island (UHI) effect, the localized thermal anomaly over the urban areas compared to nearby rural areas, is a well-known consequence of urbanization on local climate. The phenomenon was first described by Howard (1833). Three main data collection methods are typically used to establish the magnitude of the UHI: fixed stations, mobile observations and remote sensing. While the difference in air temperature at canopy level (T_c) between the city and the region beyond its periphery is the traditional definition of the UHI (ΔT_c in this study), satellite data have given rise to a new definition of UHI, i.e. the difference in surface temperature (T_s) between the urban and the rural area, viz ΔT_s.

The UHI has been described for a number of cities (Bornstein 1968; Goldreich 1992; Tso 1996; Chang and Goh 1999; Tereshchenko and Filonov 2001; Velazquez-Lozada et al. 2006; Kolokotroni and Giridharan 2008; Huang et al. 2008). However, proper quantification of the factors generating the UHI for a city has been difficult, owing to a large number of competing influences to be considered (Oke 2006). Oke (1982) gave a comprehensive overview of the possible explanations for the temperature anomaly, including the difference in albedo between the urban and the rural areas, the higher heat capacity of the urban surfaces and the difference in surface energy budget between the urban and the rural land surfaces, among other things. The significance of urban morphology and background climate on heat-island formation has been established by several empirical studies (Johnson 1985; Hogan and Ferrick 1998; Klysik and Fortuniak 1999; Steinecke 1999; Morris et al. 2001; Unger et al. 2001; Zhao et al. 2014). A recent study of ΔT_s values for 419 cities in the world found significant differences in their diurnality and inter-seasonality for different latitudes (Peng et al. 2011). This suggests that the factors influencing the heat-island in different climate zones need to be investigated further before reaching strong, generalized conclusions.

India, specially the Gangetic basin, has undergone rapid urbanization in the last few decades and currently accounts for approximately 10% of the global urban residents, second only to China (United Nations. Department of Economic and Social Affairs. Population Division 2014). Barring the last five years, studies on the UHI effect in the country have been few and far between. Moreover, a majority of the studies have been constrained to reporting the magnitude of the UHI with not much work done on understanding the influence of various factors on the urban thermal anomaly. Kanpur city (26.5°N 80.3°E), with an area of 605 km^2 and a population of 2.5 million people (United Nations Statistics Division 2013), is a representative metropolitan region in the Gangetic basin. The city experiences a humid monsoonal sub-tropical climate, with long and scorching pre-monsoons (March to June), a prolonged rainy (monsoon) season (July to September) and short winters (December to February) (Singh et al. 2004). Temperatures can fluctuate significantly from 0 °C during the winters to 47 °C during the pre-monsoons (Indian Meteorological Department 2015). During the last century, the city has developed rapidly with little planning, and represents a typical case of extreme urbanization. Figure 1 shows the land use and land cover of Kanpur city. The residential, commercial and industrial areas are centered around the city core. The western side has several educational and research institutes, while the eastern edge is dominated by agricultural fields. A detailed land-use classification of Kanpur city can also be found in Behera et al. (2011).

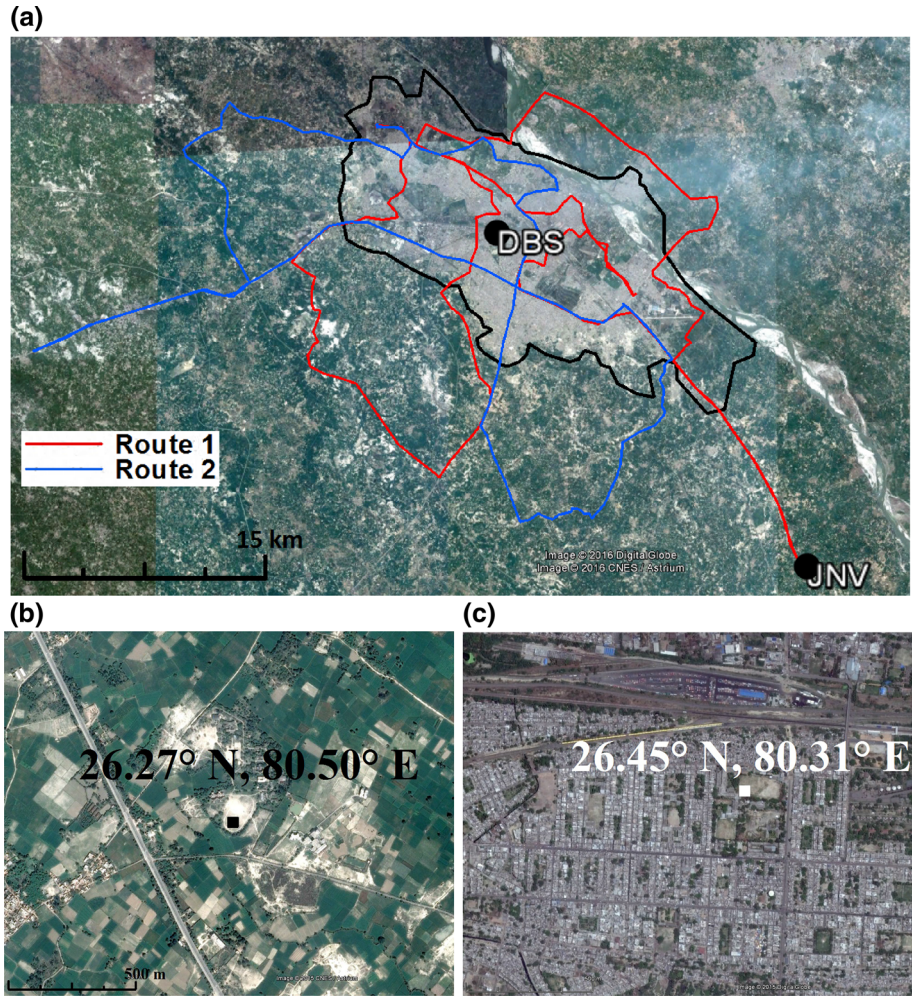

Fig. 1 Location of automatic weather stations and routes of mobile campaigns. **a** Map of Kanpur city with relative position of observational sites and routes of mobile campaigns. **b** Rural site (JNV). **c** Urban site (DBS)

The surface and canopy temperature (and thus, ΔT_c and ΔT_s), though coupled, are analyzed separately herein. This is primarily done since surface heating and canopy air heating involve different mechanisms. Jin et al. (1997) analyzed differences in skin and air temperature at various temporal and spatial scales, and found that air and skin temperatures show significant differences during the diurnal cycle. This discrepancy has also been seen in other studies (Sellers et al. 1990; Garratt 1995). For the UHI effect in particular, this can lead to differences in the diurnality and inter-seasonality of ΔT_c and ΔT_s (Jin and Shepherd 2005; Jin 2012). The surface can be assumed to be a plane, with the surface energy balance given by

$$R_{net} = H + LE + G, \tag{1}$$

where R_{net} is the net radiative flux, H is the sensible heat flux, LE is the latent heat flux and G is the soil heat flux.The latter term includes both a storage term, given by the energy stored

in the soil between the surface and the depth at which the flux is measured, and a sink term, given by the rate of energy transfer from the surface towards the deeper layers.

The net radiative flux is given by

$$R_{net} = S\downarrow + L\downarrow - S\uparrow - L\uparrow, \tag{2}$$

where $S\downarrow$ is the incoming shortwave radiative flux, $L\downarrow$ is the incoming longwave radiative flux, $S\uparrow$ is the outgoing shortwave radiative flux and $L\uparrow$ is the outgoing longwave radiative flux. It is evident that, theoretically, ΔT_s and ΔT_c, though highly correlated, should be affected differently by the various meteorological factors. This possibility has been investigated in the present study.

We have used in situ canopy and surface temperature measurements, as well as satellite estimates of land-surface temperature, to obtain ΔT_c and ΔT_s values over Kanpur, along with their diurnality and inter-seasonality. All four components of the radiative budget have been measured for both sites during the study period. These measurements have been used to tease out the urban–rural differences in the radiative budget, especially its inter-seasonal variation, and its relevance to the UHI over Kanpur. Finally, the factors moderating the inter-seasonality of the UHI have been estimated using in situ measurements, the Global Land Data Assimilation System (GLDAS) NOAH (NCEP-OSU-Air Force-Office of Hydrology) land-surface model and satellite remote sensing. Details of the measurements are presented in Sect. 2, and the diurnality and inter-seasonality of canopy and ΔT_s are illustrated in Sect. 3. Associations between the measured urban–rural radiative imbalance and ΔT_s and ΔT_c values are discussed in Sect. 4. The response of the UHI, especially its inter-seasonality, to land use and land cover is described in Sect. 5.

2 Methodology

2.1 Study Area and Site Details

Two automatic weather stations (locations in Fig. 1), one in the urban core and the other in a rural area, were used to measure air temperature, humidity, precipitation, wind speed, wind direction, $S\downarrow$, $L\downarrow$, $S\uparrow$ and $L\uparrow$ from April to September 2014. The surface temperature was derived from $L\uparrow$ assuming an emissivity of unity at both sites. The urban site lies on the playground of the Dayanand Brajendra Swarup College, which is in a dense residential section in the heart of the city. The rural site is situated 32 km away from the city centre in the playground of a rural school, Jawahar Navodaya Vidyalaya, which is surrounded by farmland.

2.2 Data Collection and Processing

A list of the sensors used at each automatic weather station is given in Table 1. Throughout the study period, all the temperature and humidity sensors were calibrated monthly against two Vaisala HMT330 temperature and humidity sensors. ΔT_c values were determined from the difference between the measured air temperature at the urban and the rural weather station at each time interval. Similarly, ΔT_s was determined from the urban–rural difference in the $L\uparrow$-derived surface temperature. The diurnal variation of air temperature and surface temperature at each site, as well as ΔT_c and ΔT_s values were calculated for the pre-monsoon and the monsoon seasons, where the pre-monsoon is considered from April to June and the monsoon from July to September. The radiative flux data (and, hence, the surface temperature) were

Table 1 List of parameters measured at each observation site

Parameter measured	Sensor make	Sensor height (m)	Sensor accuracy
Air temperature	iNGEN	1.5	$\pm 0.2\,^{\circ}$C
Relative humidity	iNGEN	1.5	$\pm .3\%$
Wind speed	iNGEN	2	± 0.5 m s^{-1}
Wind direction	iNGEN	2	$\pm 5^{\circ}$
Precipitation	iNGEN	0.5	± 3 to $\pm 5\%$
Radiation components	Kipp and Zonen	2	NA

missing at the rural site in July 2014. No interpolation was performed for the temporal and correlation analysis.

Mobile observations were carried out in the months of May (pre-monsoon), June (pre-monsoon) and September (monsoon-cloudy). Two Vaisala HMT330s were mounted on two vehicles at approximately 1.5 m from the ground and the vehicles driven at a constant speed of 40 km h^{-1}. Temperature, relative humidity and GPS data were measured at intervals of 90 s. The measurement campaigns were carried out at night, from 2200 to 0600 local time (LT), as the change in temperature with time was minimum during this period compared to any other 8 h interval during the day. The data were corrected to their values at midnight (0000 LT) using temperature trends from the fixed stations to account for the temporal temperature variation during the campaigns. Midnight was chosen as the reference time since the temporal analysis showed largest ΔT_c values at around midnight (Fig. 2). For regions traversed within the urban boundary, the urban station data were used for removing the temporal temperature trend, while the rural station data were used for locations outside the city.

MODIS TERRA (MYD11A2) 8-day nighttime land-surface temperature data (1 km $\times$ 1 km) from the same time period as the mobile campaigns were used to estimate the land-surface temperature pattern. This dataset is based on the generalized split-window algorithm (Wan 1999). The mobile measurements and satellite products give a complete spatial picture of the nighttime air temperature and surface temperature values over greater Kanpur.

For the correlation study, the urban–rural differences in radiative flux components of the surface energy balance [henceforth $\Delta(component)$] were correlated with ΔT_c and ΔT_s values for both daytime and nighttime. Here, the ΔT_s values used are the $L\uparrow$-derived surface temperature difference between the urban and the rural site. All correlations were performed with 15-min data. Before correlation, outliers (limited by mean $\pm$ 3 SD) were removed.

MODIS TERRA (MOD13Q1) 16-day enhanced vegetation index (EVI) products (250 m $\times$ 250 m) were used to investigate the variation in vegetation cover over the rural and the urban stations. The mean of four grids, i.e., an area of 500 m $\times$ 500 m, surrounding each site was used for this analysis. The enhanced vegetation index is a remotely-sensed, quantitative indicator of the quantity of biomass on the Earth's surface , and is based on the differential absorption of longwave and shortwave radiation by a vegetative canopy (Huete et al. 1999).

Global Land Data Assimilation System (GLDAS) generated data were used to estimate the latent heat flux (*LE*) over the urban and the rural sites. GLDAS is a terrestrial modeling system that drives several uncoupled land-surface models (Rodell et al. 2004). In the present study, GLDAS/NOAH version 2.7 model simulations were used. The model has been running continuously at a temporal resolution of 3 h and a global, spatial resolution of 0.25° from the

year 2000 to present and the dataset has been evaluated in previous studies (Mueller et al. 2011; Jiménez et al. 2011). In its current iteration, the NOAH land-surface model uses one canopy layer and four soil layers (Mitchell 2001), with gravity drainage at the bottom of the lowermost soil layer. The model utilizes a diurnally dependent potential temperature approach (Mahrt and Ek 1984), a simple canopy model (Pan and Mahrt 1987), a multi-layered soil model (Mahrt and Pan 1984), a bare soil evaporation scheme (Noilhan and Planton 1989), a time integration scheme (Kalnay and Kanamitsu 1988), a refined snowmelt algorithm (Koren et al. 1999), a surface runoff scheme (Schaake et al. 1996) and a thermal roughness length (Chen et al. 1997). The surface energy balance used in the NOAH land-surface model is given by Eq. 1. The bulk heat transfer equation is used to estimate H (Garratt 1993), G is estimated using Fourier's Law and LE is taken as the summation of direct soil evaporation (E_{dir}), canopy evaporation (E_c), transpiration (E_t) and sublimation from any snowpack (E_{snow}), all dependent on the Penman-derived potential evaporation formulation (E_p) (Mahrt and Ek 1984). Further detailed information on the lineage and formulations of the model can be found in Chen and Dudhia (2001). The GLDAS/NOAH model simulations used herein are forced by a combination of re-analysis and observed datasets (Rui 2011).

3 UHI Quantification

3.1 Temporal Study

Figure 2 shows the composite, diurnal plots for air temperature at both the urban and the rural sites for the pre-monsoon (a), and the monsoon (b). The same plot also shows the diurnal variation of ΔT_c, along with one standard deviation (solid vertical lines). The vertical dash-dot lines represent the mean sunrise and sunset times (to the nearest 15 min) for each season. Kanpur city shows a clear diurnality in mean ΔT_c, with higher nighttime ΔT_c values for both seasons (Fig. 2). The ΔT_c values reach a maximum value at around midnight (local time), with an average value of 3.6 ± 1.1 °C for the pre-monsoon and 2 ± 1 °C for the monsoon. The high nighttime ΔT_c value indicates that the source of this phenomenon is a difference in nighttime urban–rural surface energy balance, and is explored further in Sect. 4. Figure 3 is similar to Fig. 2, but for surface temperature and ΔT_s. The mean ΔT_s value shows no consistent difference between the pre-monsoon and the monsoon periods. While the daytime ΔT_s value is higher than nighttime ΔT_s value for the pre-monsoon, there is very little diurnal variation in ΔT_s during the monsoon (Fig. 3). Inter-seasonal differences are also seen from the temporal analysis.

The magnitude of ΔT_c is higher during the pre-monsoon for both daytime and nighttime (Fig. 2). A minimum mean value of 1.4 ± 1.2 °C is seen for the pre-monsoon and 0.5 ± 1.3 °C for the monsoon, while the peak values for the pre-monsoon and the monsoon are 8.8 and 6 °C, respectively. In other cities characterized by dry and wet periods, similar lower nocturnal magnitudes of ΔT_c have been seen during the wet season (Kim and Baik 2005; Chow and Roth 2006). Earlier studies on Delhi, also situated in the Gangetic basin, show high ΔT_c values (4–10.7 °C) during the pre-monsoon period (Mohan et al. 2013; Pandey et al. 2014). On the other hand, a previous study on Guwahati has found a lower ΔT_c magnitude of around 2.3 °C, though the inter-seasonality was similar to that seen in the present study (Borbora and Das 2014). Unlike ΔT_c, ΔT_s has higher values during the monsoon (Fig. 3). The maximum mean magnitude of ΔT_s is 3.4 ± 3.2 °C during the pre-monsoon and 5 ± 0.7 °C during the monsoon.

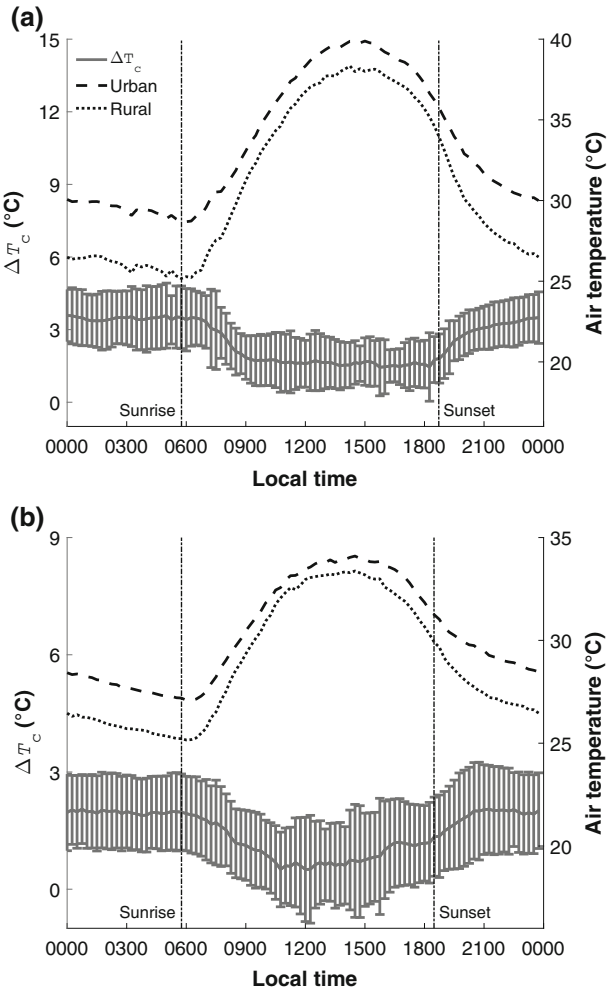

Fig. 2 Diurnal variation in the magnitude of ΔT_c for **a** dry (pre-monsoon), and **b** wet (monsoon) seasons based on diurnal, composite plots of observations. The *vertical lines* represent one standard deviation for ΔT_c every 15 min. The *dash-dot lines* represent the mean sunrise and sunset times for the season

3.2 Spatial Study

The spatial interpolation for both the campaign data and the MODIS dataset was done using residual Kriging using ArcMap 10.2.2. Residual Kriging is a stochastic spatial interpolation technique where the best-fit function is modeled as the sum of the trend component and a residual (Phillips et al. 1992). This was chosen over other spatial interpolation techniques since it shows best results for urban heat islands (and temperature profiles in general) (Dyras and Ustrnul 2007; Szymanowski and Kryza 2009). Complete satellite-derived surface temperature estimates were unavailable during the cloudy period. The missing observations also heavily bias the kriging process, as seen in Fig. 4f. The results of the mobile measurement campaigns over greater Kanpur show significant ΔT_c values surrounding the city core during

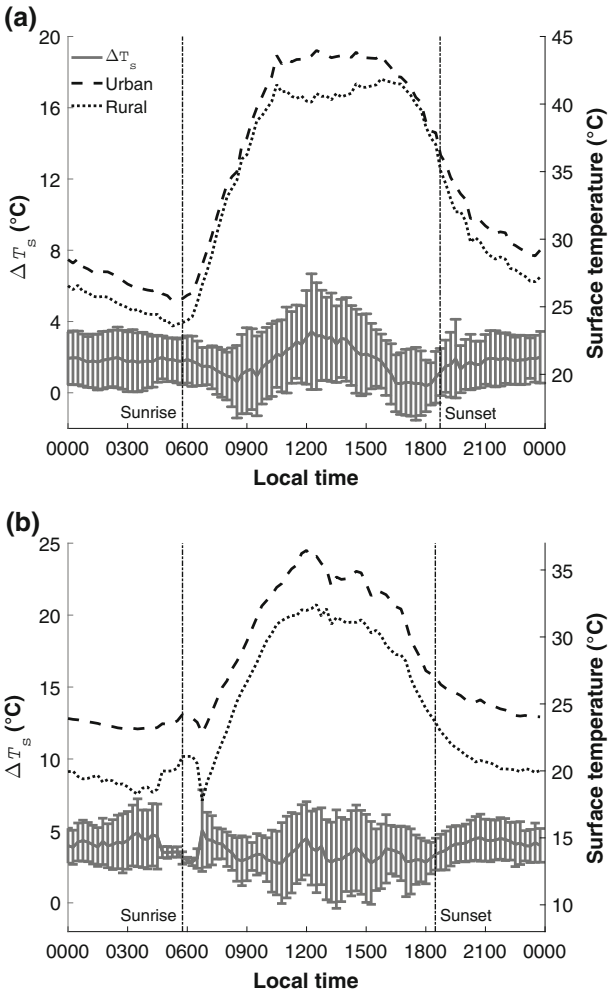

Fig. 3 Diurnal variation in the magnitude of ΔT_s for **a** dry (pre-monsoon), and **b** wet (monsoon) seasons based on diurnal, composite plots of observations. The *vertical lines* represent one SD for ΔT_s every 15 min. The *dash-dot lines* represent the mean sunrise and sunset times for the season

the pre-monsoon, with air temperature in the study area varying from 25 °C towards the edge to 32 °C in the city core (Fig. 4). The satellite-derived land-surface temperature shows that ΔT_s values between the city and its periphery have a range similar to that of ΔT_c values (Fig. 4) during this period.

Higher values are observed in the satellite observations compared to the values derived from the fixed stations (Figs. 2, 3). The urban fabric is highly heterogeneous, with different kinds of surface materials; from grassy urban parks, to concrete sidewalks and buildings, to asphalt pavements. Since asphalt and concrete have a higher heat capacity than soil, and the MODIS plots used had a resolution of 1 km $\times$ 1 km, the nighttime ΔT_s value averaged over the heterogeneous urban surface is higher than the magnitude of ΔT_s between two grassy surfaces.

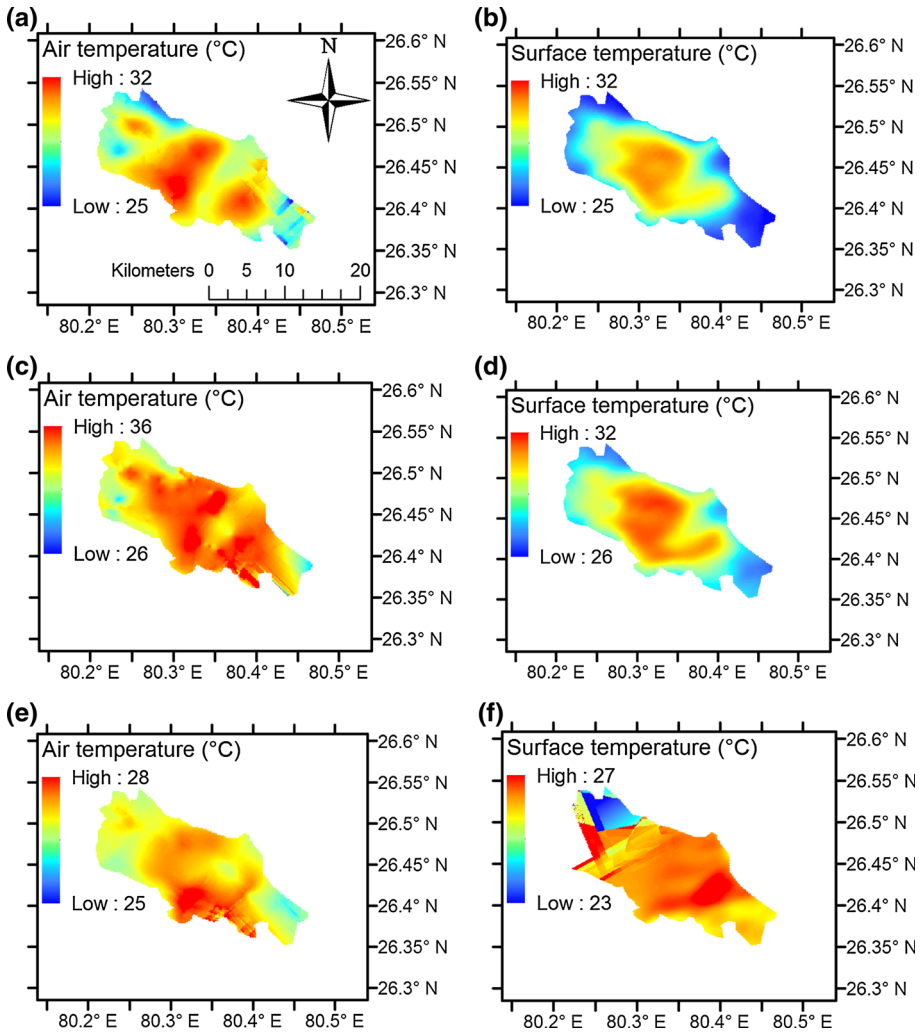

Fig. 4 Spatial pattern of air temperature over Kanpur City based on measurement campaigns on **a** 23 May 2014, **c** 6 June 2014 and, **e** 5 September 2014. Spatial characteristics of surface temperature are based on MODIS TERRA 8-day nighttime LST for **b** 17–24 May 2014, **d** 2–9 June 2014 and, **f** 29 August–5 September 2014

The results from the second measurement campaign during the pre-monsoon show similar gradient and magnitude of ΔT_c (Fig. 4). A third measurement campaign was performed during a cloudy monsoon night. The monsoon measurement campaign shows lower ΔT_c values (2–3 °C; Fig. 4) when compared to the values obtained for the pre-monsoon, which is most probably due to the presence of clouds in the monsoon (Morris et al. 2001). This corroborates the inter-seasonality observed in the temporal variation of the magnitude of ΔT_c.

In all cases, the lower temperatures are seen at the western and eastern parts, both of which have very little industrial or commercial activities. The eastern edge, in particular, shows much lower temperatures since it is dominated by agricultural fields (Fig. 1).

4 Associations Between Urban–Rural Surface Energy Differences and the Heat-Island Effect

For nighttime ΔT_c values, relatively high positive correlations are seen for $\Delta(L\uparrow)$ and $\Delta(L\downarrow)$ for both the pre-monsoon and the monsoon (Table 2). For daytime ΔT_c values, no significant association is seen except with $\Delta(L\uparrow)$. For ΔT_s, high correlations are seen for both $\Delta(L\downarrow)$ and $\Delta(L\uparrow)$ during nighttime and as compared to daytime (Table 3) . Since correlation does not necessarily imply causation, the variables showing higher correlation with the UHI are further analyzed to find inter-dependency of variables.

4.1 The Surface Urban Heat-Island

Figure 5 shows the observed diurnal variation of the four components of the radiative balance for the urban and the rural areas for both seasons, as well as the urban–rural differences in each of those terms. The bounded lines represent one standard deviation from the mean of each component for the entire season. Here, the downward direction is taken as positive for calculating R_{net}, $S\downarrow$ and $L\downarrow$, while the upward direction is considered positive for estimating $S\uparrow$ and $L\uparrow$. In the pre-monsoon, for the rural site, $S\downarrow$ reaches a maximum mean value of $750 \pm 203\,\mathrm{W\,m^{-2}}$ (mean $\pm$ one standard deviation) at around 1130 LT, while $S\uparrow$ is $169 \pm 50\,\mathrm{W\,m^{-2}}$ at the same time; $L\downarrow$ varies from a minimum of $411 \pm 24\,\mathrm{W\,m^{-2}}$ at 0600 LT to a maximum value of $484 \pm 29\,\mathrm{W\,m^{-2}}$ at 1345 LT; $L\uparrow$ is higher than $L\downarrow$, and varies from a minimum of $442 \pm 22\,\mathrm{W\,m^{-2}}$ at around 0600 LT to $558 \pm 25\,\mathrm{W\,m^{-2}}$ at around 1545 LT. For the urban site, $S\downarrow$ reaches a maximum mean value of $751 \pm 190\,\mathrm{W\,m^{-2}}$ at around 1145 LT, while $S\uparrow$ is $129 \pm 34\ \mathrm{W\,m^{-2}}$ at the same time. $L\downarrow$ varies from a minimum of

Table 2 Coefficient of determination between ΔT_c values and, urban–rural surface energy flux differences with 15-min data

Urban–rural differences in energy terms	Season			
	Pre-monsoon		Monsoon	
	Day	Night	Day	Night
Incoming shortwave	0.01	NA	0.02	NA
Incoming longwave	0.07	0.19	0.11	0.27
Outgoing shortwave	0.12	NA	0.07	NA
Outgoing longwave	0.06	0.68	0.27	0.50

Table 3 Coefficient of determination between ΔT_s values and, urban–rural surface energy flux differences with 15-min data

Urban–rural differences in energy terms	Season			
	Pre-monsoon		Monsoon	
	Day	Night	Day	Night
Incoming shortwave	Negligible	NA	0.06	NA
Incoming longwave	0.16	0.33	0.31	0.65
Outgoing shortwave	0.08	NA	Negligible	NA
Outgoing longwave	0.99	1	0.99	1

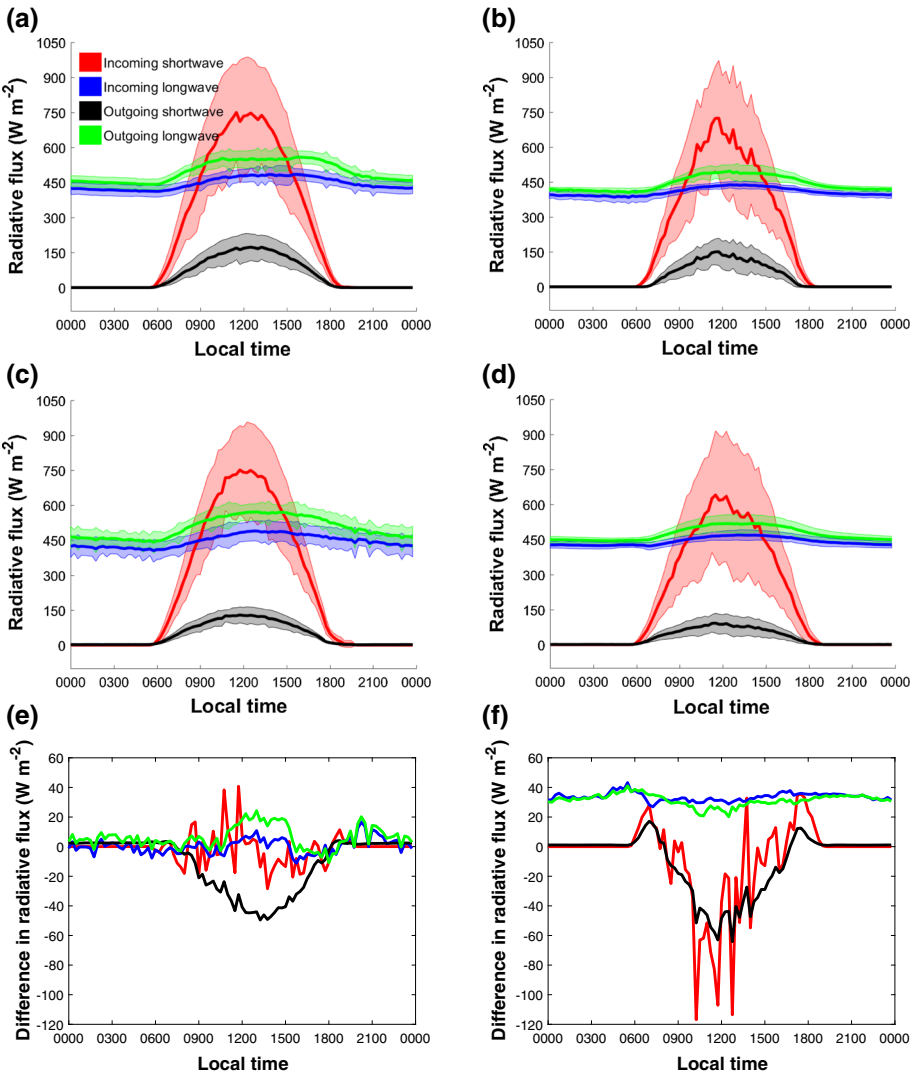

Fig. 5 Comparison of diurnal variation in radiative flux components at the two sites using diurnal, composite plots of observations. The *upper and lower bounds* represent one standard deviation of the data. **a** Pre-monsoon—rural site. **b** Monsoon—rural site. **c** Pre-monsoon—urban site. **d** Monsoon—urban site. **e** Urban–rural differences in radiative flux components—pre-monsoon **f** Urban–rural differences in radiative flux components—monsoon

$405 \pm 48\,\mathrm{W\,m^{-2}}$ at 0545 to a maximum mean value of $489 \pm 42\ \mathrm{W\,m^{-2}}$ at 1245 LT; $L\uparrow$ varies from $440 \pm 48\ \mathrm{W\,m^{-2}}$ at around 0545 LT to $571 \pm 36\,\mathrm{W\,m^{-2}}$ at around 1300 LT. All components of the radiative balance show relatively less variation at midday during the pre-monsoon, compared to the monsoon period. This is possibly due to the clear-sky conditions that prevail during this season.

Figure 6 shows the diurnal variation of the observed $\Delta(R_{net})$ and ΔT_s values. The lower albedo in the urban area (midday albedo of 0.17 at the urban site versus 0.24 at the rural site; Fig. 5) increases the $S\downarrow$ absorbed by the urban surface. The higher temperature of the

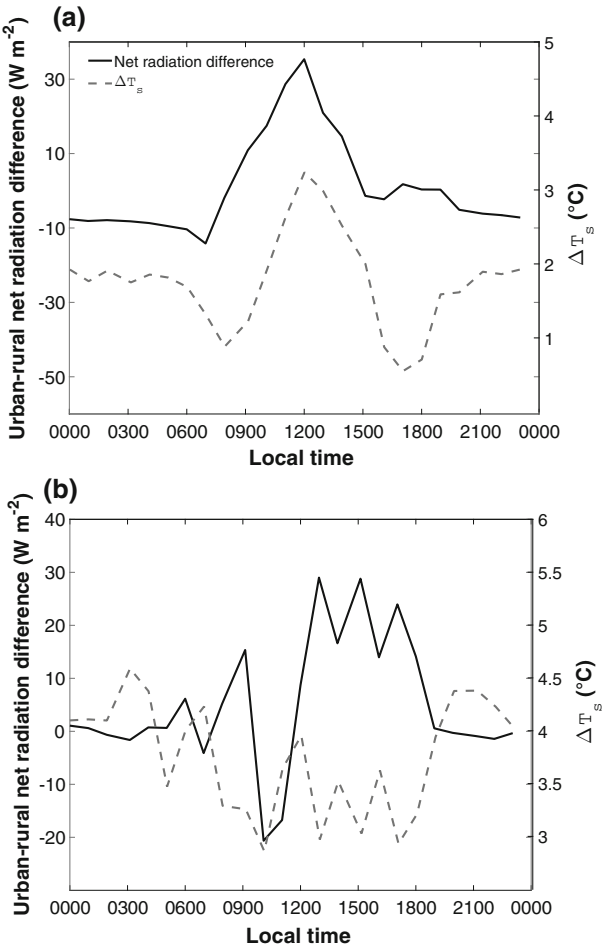

Fig. 6 Observed diurnal variation of net radiative flux difference and ΔT_s values for **a** the pre-monsoon and, **b** the monsoon

urban boundary-layer also increases $L\downarrow$ at the urban site (Wang et al. 2015). Together, this may lead to an excess R_{net} at the urban site (peak R_{net} of 563 ± 111 W m^{-2} at 1230 LT at the urban site versus 532 ± 124 W m^{-2} at the same time at the rural site), increase the surface temperature and control the trend of ΔT_s during the daytime. This is particularly apparent during the pre-monsoon season, as the daytime variation of ΔT_s closely follows $\Delta(R_{net})$ (upper panel of Fig. 6). In general, urban structures have a high thermal mass, both due to their size and the high density materials used to construct them. This property allows the urban canopy to absorb heat without any appreciable change in temperature. Thus, even if the same amount of energy is incident on both an urban and a rural area, the change in temperature of the urban canopy will be lower. Consequently, the temperature of an urban area also decreases more slowly (Goward 1981). Thus, during nighttime, the rural site cools more rapidly since the heat stored here is lower compared to the urban site. This, in addition to the higher $L\downarrow$, may lead to the nighttime ΔT_s. It should be noted that the heat capacity of the urban canopy is less of an issue for the present study. The urban site's footprint is small, and is

only partially affected by the urban surface. Thus, the canopy heat storage at both sites can be assumed to be roughly the same. However, the surrounding urban structures can increase the boundary-layer temperature above the urban area (sometimes known as the boundary-layer UHI). This higher temperature is coupled with the incoming longwave radiative flux, which in turn, increases the urban surface temperature, which is also suggested by our correlation study (Fig. 9). Overall, the diurnal trends show that the total energy released by the urban site is higher during nighttime. This can be seen in the negative $\Delta(R_{net})$ of approximately 10 W m^{-2} during the pre-monsoon nights (Fig. 6). There is no appreciable $\Delta(S\downarrow)$ during the pre-monsoon (Fig. 5). However, the $\Delta(L\uparrow)$ peaks during midday, which is a direct consequence of the peak ΔT_s at this time (Fig. 6).

During the monsoon, for both the urban and the rural sites, the diurnal trend in $S\downarrow$ is broken near midday, possibly due to interference by clouds (Fig. 5). For the rural area, maximum $S\downarrow$ and $S\uparrow$ of 724 ± 247 and 150 ± 59 W m^{-2} respectively are seen at around 1145 LT (local time). The longwave components show a trend similar to that of the pre-monsoon. $L\downarrow$ varies from a mean minimum of 384 ± 27 W m^{-2} at 0530 LT to a maximum value of 438 ± 13 W m^{-2} at 1230 LT, while $L\uparrow$ ranges from 405 ± 18 W m^{-2} at 0530 LT to 497 ± 27 W m^{-2} at 1230 LT. In the urban area, $S\downarrow$ reaches a maximum mean value of 641 ± 275 W m^{-2} at around 1130 LT, while $S\uparrow$ is 92 ± 43 W m^{-2} at the same time; $L\downarrow$ varies from 422 ± 16W m^{-2} at 0645 to a maximum mean value of 468 ± 21 W m^{-2} at 1300 LT; $L\uparrow$ varies from 444 ± 11 W m^{-2} at around 0400 LT to 518 ± 38 W m^{-2} at around 1400 LT.

Unlike the pre-monsoon, during the monsoon, $S\downarrow$ is higher at the rural site (Fig. 5), maybe because the urban area is a continuous source of high anthropogenic aerosol emissions. Thus, aerosol buildup after rainfall events over the city is rapid compared to nearby rural regions. Because of this reduced solar insolation at the urban site and the lower fraction of the $S\downarrow$ returned due to the low urban albedo, the urban–rural difference in R_{net} is less pronounced during this season (peak R_{net} of 497 ± 220 W m^{-2} at 1130 LT at the urban site versus 516 ± 161 W m^{-2} at the same time at the rural site). This increased radiative forcing due to high aerosol loading at urban sites has been seen in previous studies and may explain the observed disparity in the $\Delta(R_{net})$ between the two seasons (Carrico et al. 2003). The higher boundary-layer temperature in the urban areas may also lead to a high $L\downarrow$, while the high ΔT_s value during this season explains the significant $\Delta(L\uparrow)$ seen in Fig. 5. The diurnal trend in ΔT_s does not explicitly follow the trend in $\Delta(R_{net})$ during this season. This suggests that ΔT_s is largely controlled by the amount of energy removed from the surface during this season.

The nighttime ΔT_s value shows significant correlations with $\Delta(L\downarrow)$ ($r^2 = 0.33$ for the pre-monsoon and $r^2 = 0.65$ for the monsoon) and $\Delta(L\uparrow)$ ($r^2 = 1$ for the pre-monsoon and the monsoon) (Table 3). For daytime, the correlation is high for $\Delta(L\uparrow)$ ($r^2 = 0.99$ for the pre-monsoon and the monsoon) and lower for $\Delta(L\downarrow)$ ($r^2 = 0.16$ for the pre-monsoon and $r^2 = 0.31$ for the monsoon). It should be noted that $\Delta(L\uparrow)$ cannot solely determine ΔT_s since $L\uparrow$ is the consequence of thermal emission from the heated surface. Since both $\Delta(L\downarrow)$ and $\Delta(L\uparrow)$ show positive correlations with ΔT_s, the $\Delta(L\uparrow)$ dataset was divided into three equal bins, representing 33 percentile each, and the correlation between corresponding ΔT_s and $\Delta(L\downarrow)$ within each bin was reanalysed (Fig. 9). The analysis suggests that $\Delta(L\downarrow)$ may strongly modulate ΔT_s, especially during nighttime. During daytime, once the variability in $\Delta(L\uparrow)$ is narrowed, the relationship between $\Delta(L\downarrow)$ and ΔT_s almost disappears (not shown).

4.2 The Canopy Urban Heat-Island

As mentioned earlier, strong correlations ($r^2 = 0.68$ for the pre-monsoon and $r^2 = 0.50$ for the monsoon) were seen between the nighttime ΔT_c value and the magnitude of $\Delta(L\uparrow)$.

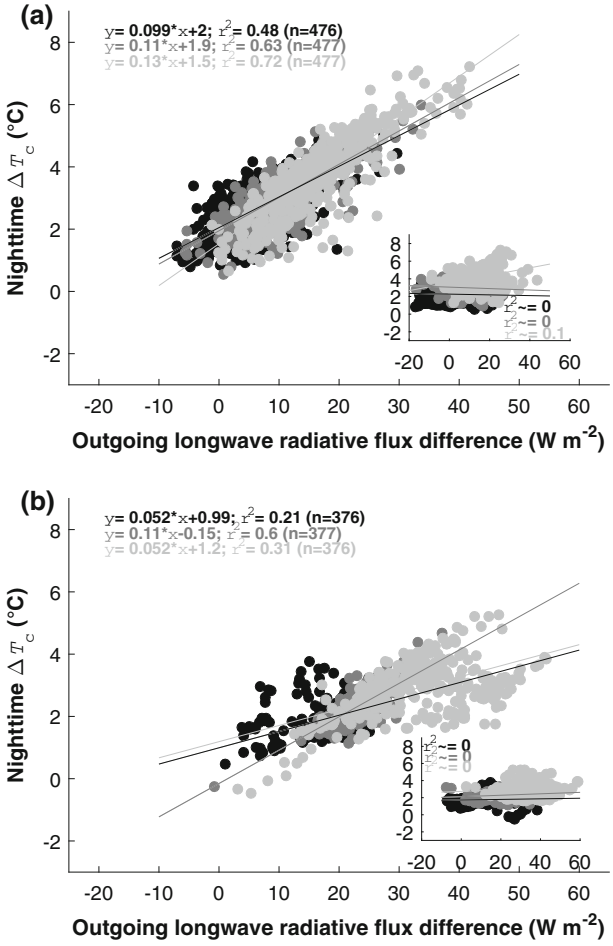

Fig. 7 Nighttime ΔT_c values versus outgoing longwave radiative flux difference for **a** the pre-monsoon and, **b** the monsoon. The *darkest points* represent the lowest 33 percentile of the incoming longwave radiative flux difference dataset while the lightest represent the highest. The *medium grey* group represents the middle 33 percentile. The plots in the *insets* show ΔT_c values plotted against the incoming longwave radiative flux difference, with outgoing longwave radiative flux difference divided into equal bins

The correlations were weaker for $\Delta(L\downarrow)$ ($r^2 = 0.19$ for the pre-monsoon and $r^2 = 0.27$ for the monsoon) (Table 2). The $\Delta(L\downarrow)$ dataset was divided into three bins, after sorting it in descending order, and the corresponding nighttime ΔT_c was correlated with $\Delta(L\uparrow)$ in each bin. This was done to restrict the variability of $\Delta(L\downarrow)$ and make the association between the nighttime ΔT_c and $\Delta(L\uparrow)$ clearer. Fig. 7 shows this linear correlation and it is consistent for all three bins for both seasons. The correlation is stronger during the pre-monsoon nights, compared to the monsoon nights. The inverse analysis was also performed, by dividing the $\Delta(L\uparrow)$ dataset into bins and correlating the nighttime ΔT_c values with the $\Delta(L\downarrow)$. Very weak relations were found (inset of Fig. 7). This implies that the high correlation initially seen between $\Delta(L\downarrow)$ and ΔT_c values (Table 2) may be due to the strong coupling between $L\downarrow$ and $L\uparrow$ in the nighttime energy budget.

As discussed above, during nighttime, $\Delta(L\uparrow)$ exists due to the ΔT_s values established during the day. Since solar radiative flux is zero and H is small, the main source of heat into the canopy air at night is due to the upwards longwave flux. $L\downarrow$ values are higher at the urban site because of the preexisting higher air temperature, both for the canopy layer and the entire urban boundary layer. Moreover, high absorbing aerosol loading in the urban area may also increase $L\downarrow$ (Zhou and Savijärvi 2014).

Wind speed has an important influence on air temperature, with advection reducing the build-up of heat and moderating temperature variances (Sodoudi et al. 2014). Urban wind speed was taken as a proxy for the advection of heat within the city, and its correlation with the urban–rural temperature difference was determined. For this analysis to be robust, the data for both day and night were segregated into six wind-direction ranges (0°–60°, 60°–120°, 120°– 180°, 180°–240°, 240°–300° and 300°–360°). In Fig. 8, the association between bin-wise segregated urban wind speed and the value of ΔT_c is shown using box plots. N represents the number of data points, μ is the mean , while σ_1 is the standard deviation in each bin. The correlation between ΔT_c magnitude and urban wind speed shows an inverse relation for all six cases (Fig. 8). This is expected since higher urban advection removes the excess heat, thus bringing down the urban air temperature, and, consequently, the ΔT_c value. High wind speeds also seem to limit the highest and lowest possible (negative) ΔT_c value, while calm conditions show a higher variability in possible ΔT_c values. This is evident from the ΔT_c standard deviation (σ_1) for the first and last bins in each wind-direction range. It is interesting to note that ΔT_c shows higher values when the rural area is downwind of the city. This, at first glance, is counterintuitive, since advection from the city to the rural area should reduce the ΔT_c magnitude. However, the rural site remains downwind of Kanpur city during the pre-monsoon and becomes upwind during the monsoon. So, the high ΔT_c values when the rural area is downwind of the city indicates the precedence of the seasonal effect over the horizontal movement of the urban heat.

4.3 Coupling of the Surface and the Canopy Heat-Islands

Previously, studies have shown associations between urban–rural longwave radiative flux differences [mainly $\Delta(L\downarrow)$] and both ΔT_c and ΔT_s values (Aida and Yaji 1979; Suckling 1981). Since direct $L\uparrow$ measurements are rare, especially for a set of nearby urban and rural stations, the same analysis has been rare for $\Delta(L\uparrow)$. The cross-analysis herein shows that though both $\Delta(L\downarrow)$ and $\Delta(L\uparrow)$ are associated with nighttime ΔT_c and the nighttime ΔT_s magnitude, $\Delta(L\downarrow)$ is associated with the magnitude of ΔT_s, while the re-radiated $\Delta(L\uparrow)$ correlates well with the magnitude of ΔT_c (Figs. 7 and 9). This relationship is very weak during the day (Tables 2 and 3).

Though there are strong, statistical associations between the magnitude of $\Delta(L\uparrow)$ and ΔT_c values, the variability in the latter may not be directly caused by variability in the former. Release of the higher energy stored in the urban structures and the different cooling rates of the urban and the rural areas may lead to the higher air temperature in the city, which would increase the urban $L\downarrow$. The higher incoming energy may further offset the radiative losses at the urban site, thus sustaining the ΔT_s value. During the study period, the 0.1-m volumetric soil moisture content of the soil at the urban site was 0.28 ± 0.13. In contrast, the rural site had a volumetric soil moisture content of 0.5 ± 0.08 at the same depth, possibly due to the effect of irrigation water from the surrounding farmland.

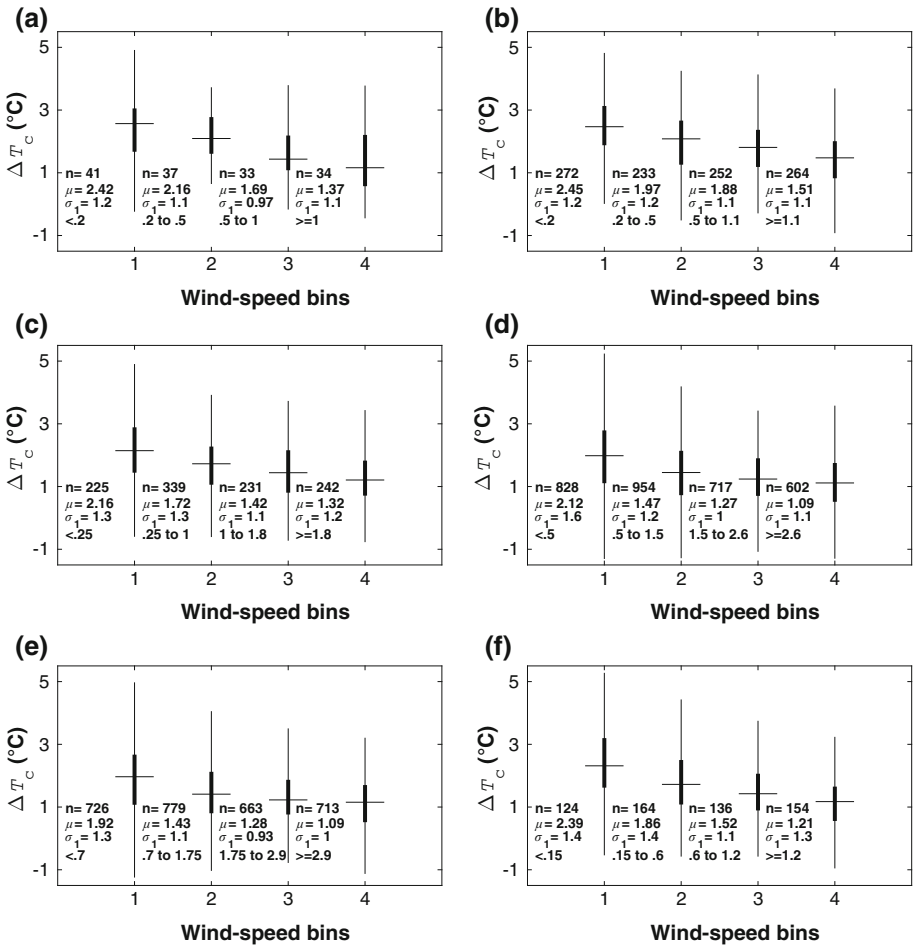

Fig. 8 Dependence of the ΔT_c magnitude on urban wind speed; *n* represents the number of data points; μ is the mean, while σ_1 is the standard deviation in each bin. The range of wind speeds (in m s^{-1}) for each bin (given below the standard deviation for each bin) was chosen to give roughly equal bins. **a** Between 0° and 60°. **b** Between 60° and 120°. **c** Between 120° and 180°. **d** Between 180° and 240°. **e** Between 240° and 300°. **f** Between 300° and 360°

The dry soil at the urban site further increases the urban–rural differences by lowering the specific heat capacity of the urban surface, allowing the urban surface temperature to rise higher, and eventually increasing the $L\uparrow$ from the urban surface. At nighttime, the boundary layer is stable and shallower than it is during daytime, restricting vertical mixing, and providing positive feedback to the ΔT_c value during nighttime (Jin 2012). During the day, other factors, such as convection and advection become more prominent. This, along with a deep, unstable daytime boundary layer, may lead to faster removal of excess urban heat from the canopy layer; thus, the low daytime magnitude of ΔT_c (Fig. 2).

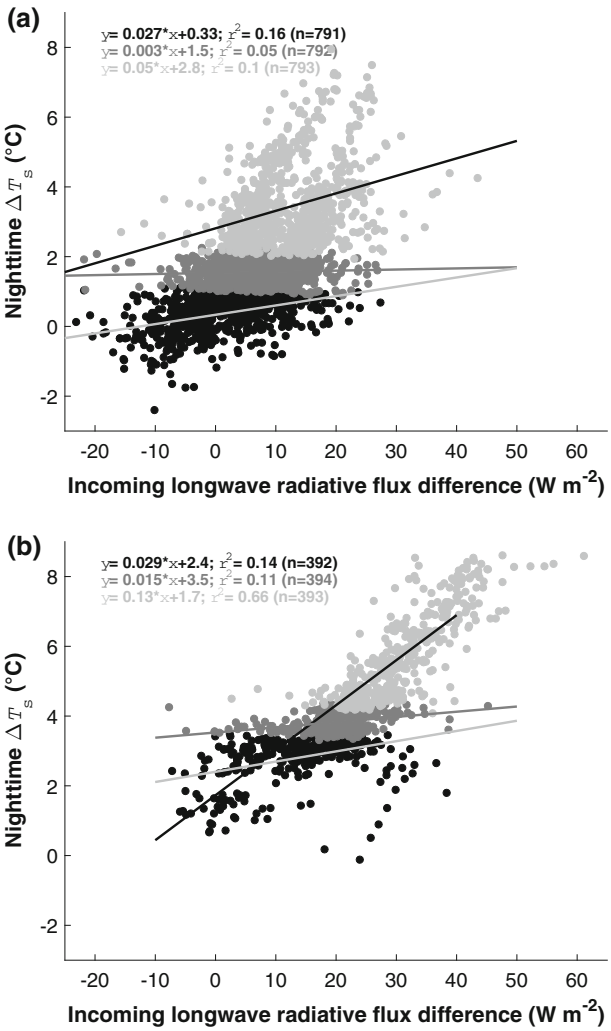

Fig. 9 Nighttime ΔT_S values versus incoming longwave radiative flux difference for **a** the pre-monsoon and, **b** the monsoon. The *darkest points* represent the lowest 33 percentile of the outgoing longwave radiative flux difference dataset while the *lightest* represent the highest. The *medium grey* group represents the middle 33 percentile

5 Rural Land-Cover Change and the Inter-Seasonality of the UHI

Figure 10 shows the variation of *EVI* (taken from MODIS MOD13Q1 products) and the 16-day running average of *LE* at 1430 LT (taken from daily 3-h GLDAS/NOAH simulations) over the urban and the rural sites during the study period. The monthly mean of the measured ΔT_S values (along with one standard deviation) is also shown. The *EVI* data are for a grid size of 500 m $\times$ 500m, while the *LE* data are for a grid size of 0.25° $\times$ 0.25° (approximately 25 km $\times$ 28 km). The *EVI* value over the urban site remains at around 0.15 from April to July, rising to a peak value of 0.3 in September, during the monsoon season. In contrast, the rural site shows a higher *EVI* value throughout the study period, as well as a higher

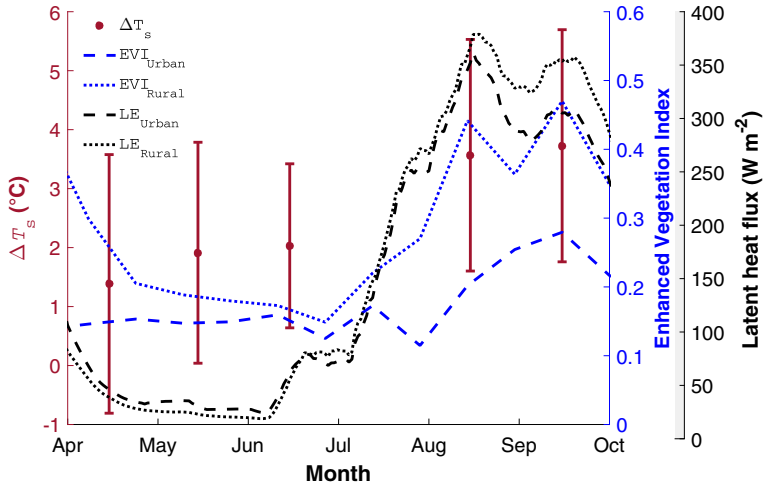

Fig. 10 Seasonal variation of enhanced vegetation index (*EVI*) over the urban and the rural station, Latent heat flux over the urban and the rural station and ΔT_s magnitude. *EVI* values represent the mean of four grid cells of 250 m × 250 m surrounding the stations for each 16-day period. *LE* values are the 16-day running averages from daily GLDAS/NOAH simulations. The ΔT_s values are the monthly means (± one standard deviation) from in situ observations

inter-seasonality of vegetation cover. It varies from 0.15 to 0.2 during the pre-monsoon and reaches a peak value of almost 0.5 in September. The *LE* values for the rural and the urban sites follow similar trends and have roughly similar magnitudes from April to the beginning of August. *LE* varies from approximately 10 W m^{-2} in June to around 200 W m^{-2} at the beginning of August. There is a significant difference in *LE* between the urban and the rural sites from August, with a maximum difference of approximately 80 W m^{-2} at the beginning of September. The rural site in the present study is surrounded by farmland, and during the pre-monsoon, the site remains relatively barren, since the rabi crops are harvested between March to April (Zhao and Siebert 2015). The decreasing trend in the rural *EVI* value seen in early April is the consequence of the harvesting. The kharif cropping season in this region begins in July to take advantage of the south-west monsoon. Moreover, there is wild, rapid growth of flora in response to the monsoon rains. Thus, there is a stark difference between the vegetation cover between the pre-monsoon and the monsoon for the rural site. While there is an inter-seasonality in the vegetation cover of the urban site, it is moderated due to the lack of irrigation patterns and externally provided irrigation water. The trend in *LE* is very similar to the trend in *EVI* values at both the sites, with greater inter-seasonality of *LE* at the rural site compared to the urban site. Studies have consistently shown that in the urban areas, heat is primarily removed through sensible heat transfer during the day (Arnfield 2003). This is primarily due to lack of pervious surfaces and more rapid surface water drainage in the urban area (Grimmond and Oke 1991). Thus, there is limited potential for evapotranspiration at the urban site (compared to the rural site) during the wet season.

The higher vegetation cover and the greater water availability due to rainfall and crop irrigation during the monsoon leads to significant evaporation at the rural site (Fig. 10), and the loss of energy from the surface may then lead to a large decrease in the rural surface temperature, compared to the urban site, establishing a large magnitude of ΔT_s. Thus, we see an increase in ΔT_s in Kanpur city with the increasing difference in *LE* (and *EVI*) between the rural and the urban site. The mean ΔT_s value varies from 1.4 ± 2.2 °C in April (dry period) to

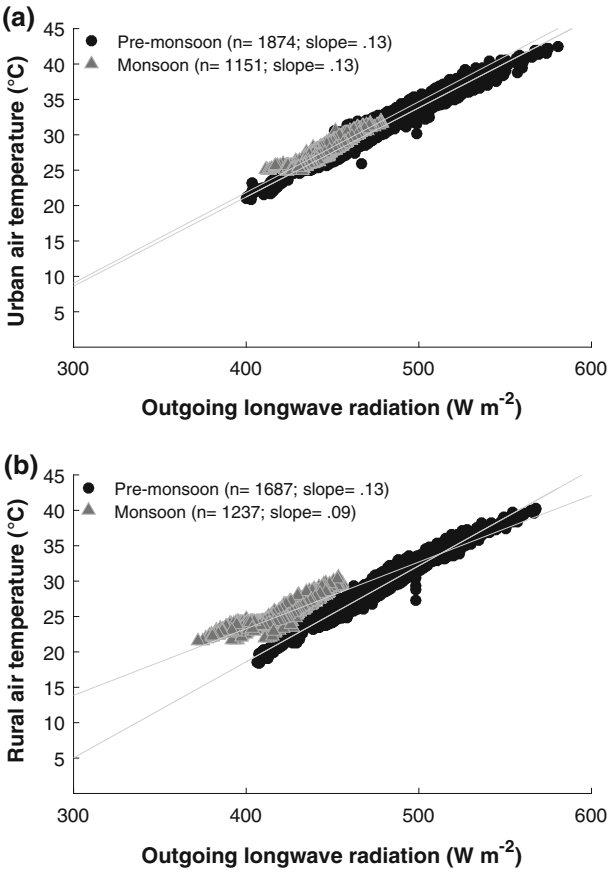

Fig. 11 Air temperature response to outgoing longwave radiative flux for **a** the urban site and, **b** the rural site

3.7±2 °C in September (wet period) (Fig. 10). Jin and Dickinson (2010) correlated nine years of MODIS-derived monthly, daytime land-surface temperature and *EVI* data for the entire globe and found a negative association between the two. It was suggested that this is due to the higher evapotranspiration over heavily vegetated regions, and land-surface temperature. A recent study around a large metropolis in Nigeria found higher ΔT_s values during the wet season compared to the dry season, and attributed the increased ΔT_s magnitude to the reduction in urban vegetation (Ayanlade 2016). Here, we suggest that the high *LE* in the rural area during the monsoon may result in a cooler rural surface and result in a greater surface temperature difference between the two locations. It is reasonable to assume that the GLDAS/NOAH derived *LE* values are overestimated in the urban grid, which has an areal extent of approximately 700 km^2, and is larger than the size of Kanpur city (roughly 400 km^2). This implies that the urban grid comprises a mix of the urban and surrounding rural areas, while the rural grid consists of mostly agricultural and rural areas. While the low resolution data used limit the present study, the results are very likely (Jin and Dickinson 2010).

Now ΔT_s and ΔT_c values have the opposite inter-seasonality, may be due to the prevalence of clouds during the monsoon period, which have been linked to lower ΔT_c values in previous studies (Suckling 1981; Morris et al. 2001; Erell and Williamson 2007; Pandey et al. 2014). Since $\Delta(L\uparrow)$ shows a strong association with ΔT_c at night, to further understand the

inter-seasonality of the ΔT_c values, the response of the canopy temperature to the ($L\uparrow$) was investigated. A greater inter-seasonal variation is seen for the rural area (Fig. 11), and can also be attributed to the seasonal land-cover changes in the rural area, due to cropping cycles and unsupervised plant growth, while the urban site remains relatively steady. The range of the values of ($L\uparrow$) is similar in both the sites for the pre-monsoon (approximately 400 W m^{-2} to 600 W m^{-2}). However, for the monsoon, the rural site shows much lower average values (as low as 370 W m^{-2} versus over 400 W m^{-2} for the urban site). Since $L\uparrow$ is proportional to the surface temperature, this supports the proposition that the high ΔT_s values during the monsoon is primarily due to the much lower temperature of the rural surface, possibly due to the higher loss of heat through evapotranspiration. The difference in response of the rural canopy temperature to ($L\uparrow$) may due to the effect of the rural canopy (and its higher inter-seasonality) on the aerodynamic and thermal properties of the canopy air. This suggests that the inter-seasonality in ΔT_c is partly controlled by the seasonal land-cover changes of the rural area.

6 Conclusions

(1) Kanpur city shows a significant magnitude of ΔT_c, mainly at night, with values higher during the pre-monsoon season (3.6 °C during the pre-monsoon versus 2 °C for the monsoon). The value of ΔT_s, on the other hand, is greater during the monsoon (5 °C during the monsoon versus 3.4 °C during the pre-monsoon). The spatial patterns of ΔT_c and ΔT_s are similar, with the ΔT_c magnitude lowest during the cloudy measurement campaign.

(2) The value of ΔT_s is associated with the magnitude of $\Delta(L\downarrow)$ during nighttime, since the surface cooling by longwave emission is greater for the urban area. Though exact attribution is difficult, the greater stored energy in urban structures, the differential cooling between the rural and the urban area, and a shallow, stable boundary layer may together establish the magnitude of ΔT_c at night.

(3) Weak associations are found between ΔT_s value and $\Delta(L\downarrow)$ for daytime. The daytime trend seen in ΔT_s during the pre-monsoon appears to be modulated by $\Delta(R_{net})$, which may be due to the effect of the lower urban surface albedo. The ΔT_c values at night persist throughout the day, but may decrease due to advection, which is more prominent during daytime.

(4) The inter-seasonality of ΔT_s is primarily ascribed to the seasonal land-cover change of the rural area. The high values during the monsoon are due to more rapid cooling of the rural surface (compared to the urban area) due to higher latent heat flux for the rural site. The effect of the rural inter-seasonality is also seen on the outgoing longwave radiative flux, which is strongly associated with the canopy air temperature.

Acknowledgements The present study was supported in part by the Department of Science and Technology, Government of India. The authors also gratefully acknowledge the financial support given by The Earth System Science Organization, Ministry of Earth Sciences, Government of India to conduct this research. The authors thank Pravin Verma and Harishankar for proper maintenance of the weather stations and for helping to organize the measurement campaigns. The authors also thank Prof. Vimal Mishra, Indian Institute of Technology, Gandhinagar, for his comments on the paper.

References

Aida M, Yaji M (1979) Observations of atmospheric downward radiation in the Tokyo area. Boundary-Layer Meteorol 16(3):453–465

Arnfield AJ (2003) Two decades of urban climate research: a review of turbulence, exchanges of energy and water, and the urban heat island. Int J Climatol 23(1):1–26
Ayanlade A (2016) Seasonality in the daytime and night-time intensity of land surface temperature in a tropical city area. Sci Total Environ 557:415–424
Behera SN, Sharma M, Dikshit O, Shukla S (2011) Development of GIS-aided emission inventory of air pollutants for an urban environment. INTECH Open Access Publisher, Rijeka
Borbora J, Das AK (2014) Summertime urban heat island study for Guwahati city, India. Sustain Cities Soc 11:61–66
Bornstein RD (1968) Observations of the urban heat island effect in New York city. J Appl Meteorol 7(4):575–582
Carrico CM, Bergin MH, Xu J, Baumann K, Maring H (2003) Urban aerosol radiative properties: measurements during the 1999 Atlanta supersite experiment. J Geophys Res Atmos (1984–2012) 108(D7):8422
Chang CH, Goh KC (1999) The relationship between height to width ratios and the heat island intensity at 22:00 h for Singapore. Int J Climatol 19(9):1011–1023
Chen F, Dudhia J (2001) Coupling an advanced land surface-hydrology model with the Penn State-NCAR MM5 modeling system. part I: model implementation and sensitivity. Mon Weather Rev 129(4):569–585
Chen F, Janjić Z, Mitchell K (1997) Impact of atmospheric surface-layer parameterizations in the new land-surface scheme of the NCEP mesoscale eta model. Boundary-Layer Meteorol 85(3):391–421
Chow WT, Roth M (2006) Temporal dynamics of the urban heat island of Singapore. Int J Climatol 26(15):2243–2260
Dyras I, Ustrnul Z (2007) The spatial analysis of the selected meteorological fields in the example of Poland. Spatial interpolation for climate data: the use of GIS in climatology and meteorology, 87–96
Erell E, Williamson T (2007) Intra-urban differences in canopy layer air temperature at a mid-latitude city. Int J Climatol 27(9):1243–1255
Garratt JR (1993) Sensitivity of climate simulations to land-surface and atmospheric boundary-layer treatments—a review. J Clim 6(3):419–448
Garratt JR (1995) Observed screen (air) and gcm surface/screen temperatures: implications for outgoing longwave fluxes at the surface. J Clim 8(5):1360–1368
Goldreich Y (1992) Urban climate studies in Johannesburg, a sub-tropical city located on a ridge—a review. Atmos Environ Part B Urban Atmos 26(3):407–420
Goward SN (1981) Thermal behavior of urban landscapes and the urban heat island. Phys Geogr 2(1):19–33
Grimmond CSB, Oke TR (1991) An evapotranspiration-interception model for urban areas. Water Resour Res 27(7):1739–1755
Hogan AW, Ferrick MG (1998) Observations in nonurban heat islands. J Appl Meteorol 37(2):232–236
Howard L (1833) The climate of London: deduced from meteorological observations made in the metropolis and at various places around it, vol 2. Harvey and Darton, J. and A. Arch, Longman, Hatchard, S. Highley [and] R. Hunter
Huang L, Li J, Zhao D, Zhu J (2008) A fieldwork study on the diurnal changes of urban microclimate in four types of ground cover and urban heat island of Nanjing, China. Build Environ 43(1):7–17
Huete A, Justice C, Van Leeuwen W (1999) Modis vegetation index (mod13). Algorithm Theor Basis Doc 3:213
Indian Meteorological Department (2015) Ever recorded maximum and minimum temperatures up to 2010. http://www.imdpune.gov.in/Temp_Extremes/histext2010.pdf. Accessed 2 May 2015
Jiménez C, Prigent C, Mueller B, Seneviratne S, McCabe M, Wood E, Rossow W, Balsamo G, Betts A, Dirmeyer P et al (2011) Global intercomparison of 12 land surface heat flux estimates. J Geophys Res Atmos 116(D2)
Jin M, Dickinson RE (2010) Land surface skin temperature climatology: benefitting from the strengths of satellite observations. Environ Res Lett 5(4):044,004
Jin M, Shepherd JM (2005) Inclusion of urban landscape in a climate model: How can satellite data help? Bull Am Meteorol Soc 86(5):681–689
Jin M, Dickinson R, Vogelmann A (1997) A comparison of CCM2-bats skin temperature and surface-air temperature with satellite and surface observations. J Clim 10(7):1505–1524
Jin MS (2012) Developing an index to measure urban heat island effect using satellite land skin temperature and land cover observations. J Clim 25(18):6193–6201
Johnson D (1985) Urban modification of diurnal temperature cycles in Birmingham, UK. Int J Climatol 5(2):221–225
Kalnay E, Kanamitsu M (1988) Time schemes for strongly nonlinear damping equations. Mon Weather Rev 116(10):1945–1958
Kim YH, Baik JJ (2005) Spatial and temporal structure of the urban heat island in Seoul. J Appl Meteorol 44(5):591–605

Klysik K, Fortuniak K (1999) Temporal and spatial characteristics of the urban heat island of Lodz, Poland. Atmos Environ 33:3885–3895
Kolokotroni M, Giridharan R (2008) Urban heat island intensity in London: an investigation of the impact of physical characteristics on changes in outdoor air temperature during summer. Sol Energy 82(11):986–998
Koren V, Schaake J, Mitchell K, Duan QY, Chen F, Baker J (1999) A parameterization of snowpack and frozen ground intended for NCEP weather and climate models. J Geophys Res Atmos (1984–2012) 104(D16):19,569–19,585
Mahrt L, Ek M (1984) The influence of atmospheric stability on potential evaporation. J Clim Appl Meteorol 23:222
Mahrt L, Pan H (1984) A two-layer model of soil hydrology. Boundary-Layer Meteorol 29(1):1–20
Mitchell K (2001) The community Noah land-surface model (LSM). User's Guide, Public Release Version 2(7):1
Mohan M, Kikegawa Y, Gurjar B, Bhati S, Kolli NR (2013) Assessment of urban heat island effect for different land use-land cover from micrometeorological measurements and remote sensing data for megacity Delhi. Theor Appl Climatol 112(3–4):647–658
Morris C, Simmonds I, Plummer N (2001) Quantification of the influences of wind and cloud on the nocturnal urban heat island of a large city. J Appl Meteorol 40(2):169–182
Mueller B, Seneviratne S, Jimenez C, Corti T, Hirschi M, Balsamo G, Ciais P, Dirmeyer P, Fisher J, Guo Z et al (2011) Evaluation of global observations-based evapotranspiration datasets and IPCC AR4 simulations. Geophys Res Lett 38(6):L06402
Noilhan J, Planton S (1989) A simple parameterization of land surface processes for meteorological models. Mon Weather Rev 117(3):536–549
Oke TR (1982) The energetic basis of the urban heat island. Q J R Meteorol Soc 108(455):1–24
Oke TR (2006) Towards better scientific communication in urban climate. Theor Appl Climatol 84(1–3):179–190
Pan HL, Mahrt L (1987) Interaction between soil hydrology and boundary-layer development. Boundary-Layer Meteorol 38(1–2):185–202
Pandey AK, Singh S, Berwal S, Kumar D, Pandey P, Prakash A, Lodhi N, Maithani S, Jain VK, Kumar K (2014) Spatio-temporal variations of urban heat island over Delhi. Urban Clim 10:119–133
Peng S, Piao S, Ciais P, Friedlingstein P, Ottle C, Breon FM, Nan H, Zhou L, Myneni RB (2011) Surface urban heat island across 419 global big cities. Environ Sci Technol 46(2):696–703
Phillips DL, Dolph J, Marks D (1992) A comparison of geostatistical procedures for spatial analysis of precipitation in mountainous terrain. Agric For Meteorol 58(1):119–141
Rodell M, Houser P, Uea Jambor, Gottschalck J, Mitchell K, Meng C, Arsenault K, Cosgrove B, Radakovich J, Bosilovich M et al (2004) The global land data assimilation system. Bull Am Meteorol Soc 85(3):381–394
Rui H (2011) Readme document for global land data assimilation system version 1 (gldas-1). Products at http://disc.sci.gsfc.nasa.gov/services/grads-gds/gldas
Schaake JC, Koren VI, Duan QY, Mitchell K, Chen F (1996) Simple water balance model for estimating runoff at different spatial and temporal scales. J Geophys Res D Atmos 101:7461–7475
Sellers P, Rasool S, Bolle H (1990) A review of satellite data algorithms for studies of the land surface. Bull Am Meteorol Soc 71(10):1429–1447
Singh R, Dey S, Tripathi S, Tare V, Holben B (2004) Variability of aerosol parameters over Kanpur, northern India. J Geophys Res Atmos (1984–2012) 109(D23)
Sodoudi S, Shahmohamadi P, Vollack K, Cubasch U, Che-Ani A (2014) Mitigating the urban heat island effect in megacity Tehran. Adv Meteorol
Steinecke K (1999) Urban climatological studies in the Reykjavık subarctic environment, Iceland. Atmos Environ 33(24):4157–4162
Suckling PW (1981) Nocturnal observations of incoming longwave radiation and the urban heat island for a small Prairie city. Arch Meteorol Geophys Bioklim Ser B 29(1–2):23–27
Szymanowski M, Kryza M et al (2009) GIS-based techniques for urban heat island spatialization. Clim Res 38(2):171
Tereshchenko I, Filonov A (2001) Air temperature fluctuations in Guadalajara, Mexico, from 1926 to 1994 in relation to urban growth. Int J Climatol 21(4):483–494
Tso C (1996) A survey of urban heat island studies in two tropical cities. Atmos Environ 30(3):507–519
Unger J, Sümeghy Z, Zoboki J (2001) Temperature cross-section features in an urban area. Atmos Res 58(2):117–127
United Nations Department of Economic and Social Affairs Population Division (2014) World urbanization prospects: The 2014 revision, UN

United Nations Statistics Division (2013) Demographic yearbook. http://unstats.un.org/unsd/demographic/products/dyb/dybsets/2013.pdf. Accessed 2 May 2015

Velazquez-Lozada A, Gonzalez JE, Winter A (2006) Urban heat island effect analysis for San Juan, Puerto Rico. Atmos Environ 40(9):1731–1741

Wan Z (1999) Modis land-surface temperature algorithm theoretical basis document (lst atbd). Institute for Computational Earth System Science, Santa Barbara

Wang L, Gao Z, Miao S, Guo X, Sun T, Liu M, Li D (2015) Contrasting characteristics of the surface energy balance between the urban and rural areas of Beijing. Adv Atmos Sci 32(4):505–514

Zhao G, Siebert S (2015) Season-wise irrigated and rainfed crop areas for india around year 2005. doi:10.13019/M2CC71. https://mygeohub.org/publications/11

Zhao L, Lee X, Smith RB, Oleson K (2014) Strong contributions of local background climate to urban heat islands. Nature 511(7508):216–219

Zhou Y, Savijärvi H (2014) The effect of aerosols on long wave radiation and global warming. Atmos Res 135:102–111